

Electron-Phonon Systems on a Universal Quantum Computer

Alexandru Macridin, Panagiotis Spentzouris, James Amundson, Roni Harnik
Fermilab, P.O. Box 500, Batavia, Illinois 60510, USA

We present an algorithm that extends existing quantum algorithms for simulating fermion systems in quantum chemistry and condensed matter physics to include bosons in general and phonons in particular. We introduce a qubit representation for the low-energy subspace of phonons which allows an efficient simulation of the evolution operator of the electron-phonon systems. As a consequence of the Nyquist-Shannon sampling theorem, the phonons are represented with exponential accuracy on a discretized Hilbert space with a size that increases linearly with the cutoff of the maximum phonon number. The additional number of qubits required by the presence of phonons scales linearly with the size of the system. The additional circuit depth is constant for systems with finite-range electron-phonon and phonon-phonon interactions and linear for long-range electron-phonon interactions. Our algorithm for a Holstein polaron problem was implemented on an Atos Quantum Learning Machine (QLM) quantum simulator employing the Quantum Phase Estimation method. The energy and the phonon number distribution of the polaron state agree with exact diagonalization results for weak, intermediate and strong electron-phonon coupling regimes.

Introduction. The algorithms for simulating many-fermion systems on quantum computers have progressed tremendously in recent years [1–9]. Due to the relatively small amount of resources required, near-future quantum simulations of strongly-correlated electrons are expected to have significant scientific impact in quantum chemistry and condensed matter physics. In this letter and in Ref. [10] we extend the existing fermion algorithms to include bosons, opening up the possibility for quantum simulation to whole new classes of physical systems.

The electron-phonon model is an example of non-relativistic quantum field theory. The phonons are the most common bosonic excitations in solids. Their interaction with electrons can significantly renormalize the electric and transport properties of materials or can lead to dramatic effects, such as superconductivity or Jahn-Teller distortions. Moreover, the interaction of electrons with other bosonic collective excitations in solids (such as spin, orbital, charge, etc.) can be addressed by similar Hamiltonians.

While there are established ways to map fermion states to qubits [3, 6, 11], much less is discussed about bosons. In Ref. [12] bosons are represented as a sum of n_x parafermions (qubits), up to an error $\mathcal{O}(n/n_x)$, where n is the boson state occupation number. This requires a large number of qubits, especially in the intermediate and strong coupling regimes where n is large. In Refs. [5, 13] systems with a fixed number of bosons are addressed, but the method is not suitable to fermion-boson interacting systems where the number of bosons is not conserved. An algorithm for calculating scattering amplitudes in quantum field theories, based on the discretization of the continuous field value at each lattice site has been proposed in Ref. [14]. In their approach the required number of qubits scales as $\log(1/\epsilon)$, whereas in our scales exponentially faster, $\approx \log(\log(1/\epsilon))$, where ϵ is the desired accuracy. We find that only a small number of additional qubits per site, $n_x \approx 6$ or 7, is enough to

simulate weak, intermediate, and strong coupling regimes of most electron-phonon problems of interest.

We treat the phonons as a finite set of harmonic oscillators (HO). We show that the low-energy space of a HO is, up to an exponentially small error, isomorphic with the low-energy subspace of a finite-sized Hilbert space. Similar finite-sized Hilbert space truncation is employed by the Fourier grid Hamiltonian (FGH) method [15] and is related to more general discrete variable representation (DVR) methods [16–18]. We present a novel explanation for the exponential accuracy of the FGH method based on the Nyquist-Shannon (NS) sampling theorem [19]. The finite-sized phonon Hilbert space is mapped onto the qubit space of universal quantum computers. The size of the low-energy subspace is given by the maximum phonon number cutoff; the size of the truncated space increases linearly with this cutoff. The number of qubits necessary to store phonons scales logarithmically with the cutoff and linearly with the system size N . The electrons are mapped to qubit states via the Jordan-Wigner transformation [3, 6, 20]. The algorithm simulates the evolution operator of the electron-phonon Hamiltonian. For long-range interactions, the additional circuit depth and the number of gates due to the inclusion of phonons is at worst $\mathcal{O}(N^2)$, while for finite-range interactions the additional circuit depth is constant.

We benchmark our algorithm by running a simulation of the two-site Holstein polaron [21] utilizing the Quantum Phase Estimation (QPE) method [2, 22–26] on an Atos Quantum Learning Machine (QLM) simulator. The energy and phonon distribution of the polaron state agree with results obtained from exact diagonalization.

The electron-phonon model. The Hamiltonian is

$$H = H_e + H_p + H_{ep}, \quad (1)$$

with

$$H_e = \sum_{ij} t_{ij} (c_i^\dagger c_j + c_j^\dagger c_i) + \sum_{ijkl} U_{ijkl} c_i^\dagger c_j^\dagger c_k c_l, \quad (2)$$

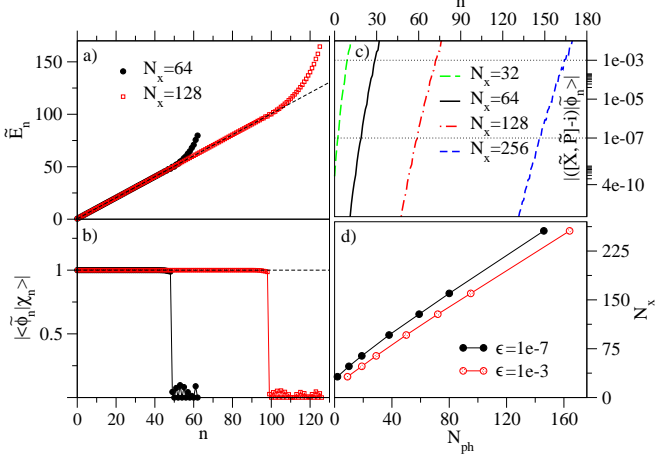


FIG. 1. (a) Eigenspectrum \tilde{E}_n of \tilde{H}_h (17) for $N_x = 64$ and $N_x = 128$. (b) Overlap between the eigenvectors $|\tilde{\phi}_n\rangle$ of \tilde{H}_h , and $|\chi_n\rangle$ (Eq.(9)). (c) $|([\tilde{X}, \tilde{P}] - i)|\tilde{\phi}_n\rangle|$ versus n for different values of N_x . For $n < N_{ph}$ where N_{ph} is a cutoff number increasing with increasing N_x , $\tilde{E}_n = n + \frac{1}{2} + \epsilon$, $|\tilde{\phi}_n\rangle = |\chi_n\rangle + \epsilon$ and $[\tilde{X}, \tilde{P}]|\tilde{\phi}_n\rangle = i|\tilde{\phi}_n\rangle + \epsilon$, with $|\epsilon| \lesssim 10 \exp[-0.51N_x(1 - 1.5N_{ph}/N_x)]$. (d) The size of the discrete space, N_x , increases linearly with the size of the low-energy subspace, N_{ph} . The full (open) symbols are extracted from (c) for $\epsilon = 10^{-7}$ ($\epsilon = 10^{-3}$).

$$H_p = \sum_{n\nu} \frac{P_{n\nu}^2}{2M_\nu} + \frac{1}{2} M_\nu \omega_{n\nu}^2 X_{n\nu}^2 + \sum_{n\nu m\mu} K_{n\nu m\mu} X_{n\nu} X_{m\mu}, \quad (3)$$

$$H_{ep} = \sum_{ij n\nu} g_{ij n\nu} \left(c_i^\dagger c_j + c_j^\dagger c_i \right) X_{n\nu}, \quad (4)$$

where H_e (H_p) contains electronic (phononic) degrees of freedom and H_{ep} describes the electron-phonon interaction. The sums are taken over the electron orbitals (i, j, k, l), ion positions (m, n) and vibrational modes (μ, ν).

Phonon space truncation. The phonons in Eq.(1) are described by a set of HOs. The phonon Hilbert space is a direct product of HO spaces. Below we address the truncation of the HO space on a finite-sized space.

The HO Hamiltonian is $H_h = P^2/2 + X^2/2$, where the operators X , P and H_h are rescaled by $1/\sqrt{M\omega}$, $\sqrt{M\omega}$ and $1/\omega$, respectively. The eigenspectrum and the eigenvectors in the position basis are

$$E_n = n + \frac{1}{2}, \quad \langle x|\phi_n\rangle \equiv \phi_n(x) = \frac{1}{\pi^{\frac{1}{4}} \sqrt{2^n n!}} e^{-\frac{x^2}{2}} H_n(x). \quad (5)$$

The Hermite-Gauss (HG) functions $\phi_n(x)$ are also eigenfunctions of the Fourier transform operator [27],

$$[\mathcal{F}(\phi_n)](p) \equiv \hat{\phi}_n(p) = (-i)^n \phi_n(p). \quad (6)$$

and satisfy

$$x\phi_n(x) = (\sqrt{n+1}\phi_{n+1}(x) + \sqrt{n}\phi_{n-1}(x)) / \sqrt{2} \quad (7)$$

$$p\hat{\phi}_n(p) = i \left(\sqrt{n+1}\hat{\phi}_{n+1}(p) - \sqrt{n}\hat{\phi}_{n-1}(p) \right) / \sqrt{2}. \quad (8)$$

The equations (7) and (8) are the eigenvalue equations for the position $X = (b^\dagger + b) / \sqrt{2}$ and momentum $P = i(b^\dagger - b) / \sqrt{2}$ operators, where b^\dagger (b) is the creation (annihilation) operator.

The HG functions fall exponentially fast to zero for large argument. For any positive integer cutoff N_{ph} , a half-width L can be chosen such that for all $n < N_{ph}$, $|\hat{\phi}_n(p)| < \epsilon$ for $|p| > L$ and $|\phi_n(x)| < \epsilon$ for $|x| > L$, where $\epsilon \propto \exp(-L^2/2)$. With exponentially good accuracy we can restrict to the region $|p| < L$ and $|x| < L$. The NS sampling theorem [19] states that, without loss of information, $\phi_n(x)$ can be sampled at points $x_i = i\Delta$, where i is an integer and $\Delta = \pi/L$. We can restrict i to N_x sampling points, $i = \overline{-N_x/2, N_x/2 - 1}$, such that $|x| < L$. This implies $2L = N_x\Delta = \sqrt{2\pi N_x}$ [10].

Let us consider the N_x finite-sized subspace, $\tilde{\mathcal{H}}$, spanned by the sampling position vectors $\{|x_i\rangle\}_i$, and define the vectors $|\chi_n\rangle \in \tilde{\mathcal{H}}$ by

$$\langle x_i|\chi_n\rangle \equiv \sqrt{\Delta}\phi_n(x_i). \quad (9)$$

As a consequence of the NS theorem [10], the vectors $\{|\chi_n\rangle\}_{n < N_{ph}}$ are orthonormal and

$$\langle p_m|\chi_n\rangle = \sqrt{2\pi\Delta}\hat{\phi}_n(p_m), \quad (10)$$

where $|p_m\rangle = N_x^{-1/2} \sum_{i=-\frac{N_x}{2}}^{\frac{N_x}{2}-1} e^{ix_i p_m} |x_i\rangle$. In Eq.(10) $\hat{\phi}_n(p_m)$ is the HG function in the momentum representation (Eq.(6)) sampled at $p_m = m\Delta$ with $m = \overline{-N_x/2, N_x/2 - 1}$.

Since $\langle x_i|\chi_n\rangle \propto \phi_n(x_i)$ and $\langle p_m|\chi_n\rangle \propto \hat{\phi}_n(p_m)$, Eqs.(7), (8), (9) and (10) imply

$$x_i \langle x_i|\chi_n\rangle = (\sqrt{n+1}\langle x_i|\chi_{n+1}\rangle + \sqrt{n}\langle x_i|\chi_{n-1}\rangle) / \sqrt{2}, \quad (11)$$

$$p_m \langle p_m|\chi_n\rangle = i(\sqrt{n+1}\langle p_m|\chi_{n+1}\rangle - \sqrt{n}\langle p_m|\chi_{n-1}\rangle) / \sqrt{2}, \quad (12)$$

for $n < N_{ph}$. If we define the operators

$$\tilde{X}|\chi_n\rangle = x_i|\chi_n\rangle, \quad (13)$$

$$\tilde{P}|\chi_n\rangle = p_m|\chi_n\rangle, \quad (14)$$

acting on $\tilde{\mathcal{H}}$, Eqs.(11) and (12) read

$$\tilde{X}|\chi_n\rangle = (\sqrt{n+1}|\chi_{n+1}\rangle + \sqrt{n}|\chi_{n-1}\rangle) / \sqrt{2}, \quad (15)$$

$$\tilde{P}|\chi_n\rangle = i(\sqrt{n+1}|\chi_{n+1}\rangle - \sqrt{n}|\chi_{n-1}\rangle) / \sqrt{2}, \quad (16)$$

which implies $[\tilde{X}, \tilde{P}]|\chi_n\rangle = i|\chi_n\rangle$ for $n < N_{ph}$. On the subspace spanned by $\{|\chi_n\rangle\}_{n < N_{ph}}$ one has $[\tilde{X}, \tilde{P}] = i$.

Therefore the algebra generated by \tilde{X} and \tilde{P} is isomorphic with the algebra generated by X and P on the harmonic oscillator subspace spanned by $\{|\phi_n\rangle\}_{n < N_{ph}}$.

The vectors $\{|\chi_n\rangle\}_{n < N_{ph}}$ are eigenvectors of

$$\tilde{H}_h = \tilde{P}^2/2 + \tilde{X}^2/2, \quad (17)$$

satisfying $\tilde{H}_h|\chi_n\rangle = (n + 1/2)|\chi_n\rangle$. Moreover, they span the low-energy subspace of \mathcal{H} , as the numerical investigation presented below shows.

The eigenspectrum \tilde{E}_n of \tilde{H}_h calculated by exact diagonalization is shown in Fig. 1(a). The first N_{ph} energy levels are the same as the corresponding HO energy levels, *i.e.*, $\tilde{E}_n = n + 1/2 + \epsilon$. The eigenstates $\{|\phi_n\rangle\}_{n < N_{ph}}$ of \tilde{H}_h are the projected HG functions on the discrete basis $\{|\chi_n\rangle\}_{n < N_{ph}}$, Eq.(9). This can be inferred from Fig. 1(b) where we see that the overlap $|\langle\tilde{\phi}_n|\chi_n\rangle| = 1 - \epsilon$ for $n < N_{ph}$. Fig. 1(c) shows that $|([\tilde{X}, \tilde{P}] - i)|\tilde{\phi}_n\rangle| < \epsilon$ for $n < N_{ph}$. The value of ϵ is exponentially small, a consequence of cutting the tails of the HG functions for $|x|, |p| > L$. Numerically, we find $|\epsilon| \lesssim 10 \exp[-0.51N_x(1 - 1.5N_{ph}/N_x)]$. The numerical results agree with the analytical predictions, supporting the isomorphism between the $\{\tilde{X}, \tilde{P}\}$ and the $\{X, P\}$ algebras on the low-energy subspace defined by $n < N_{ph}$.

The size N_x of \mathcal{H} increases approximately linearly with increasing N_{ph} . In Fig. 1(d) we plot the minimum N_x necessary to have N_{ph} states in the low-energy regime with $\epsilon = 10^{-7}$ and $\epsilon = 10^{-3}$ accuracy. The proportionality between N_x and N_{ph} is a consequence of the relations $L_{N_{ph}} \propto \sqrt{N_{ph}}$ [10] and $L_{N_{ph}} \propto \sqrt{N_x}$.

As long as the physics can be addressed by truncating the number of phonons per state our finite-sized representation is suitable for computation. The cutoff N_{ph} increases with increasing effective strength of interaction. For stable systems the truncation errors are expected to converge quickly to zero with increasing N_{ph} [10].

Algorithm. Our algorithm simulates the evolution operator $\exp(-iHt)$ on a gate quantum computer. We employ the Trotter-Suzuki expansion [28, 29] of $\exp(-iHt)$ to a product of short-time evolution operators corresponding to the noncommuting terms in the Hamiltonian.

On a gate quantum computer each HO state is represented as a superposition of N_x discrete states $\{|x\rangle\}$ and stored on a register of $n_x = \log_2 N_x$ qubits. The operators X and P are replaced by their discrete versions \tilde{X} (Eq.(13)) and \tilde{P} (Eq.(14)), respectively. The following equations are true: $\tilde{X}|x\rangle = \tilde{x}|x\rangle$ and $\tilde{P}|p\rangle = \tilde{p}|p\rangle$, where $\{|p\rangle\}$ are obtained from $\{|x\rangle\}$ via the discrete Fourier transform. The eigenvalues are $\tilde{x} = (x - N_x/2)\Delta$ and $\tilde{p} = [(p + N_x/2) \bmod N_x - N_x/2]\Delta$. They are different from the ones in Eqs. (13) and (14) since the stored states in the qubit registers are numbers between 0 and $N_x - 1$ and not between $-N_x/2$ and $N_x/2 - 1$.

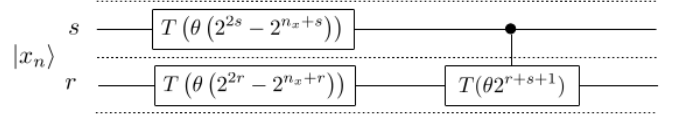


FIG. 2. The circuit $|x_n\rangle \rightarrow \exp(i2^{n_x-2}\theta)\exp[-i(x_n - 2^{n_x-1})^2\theta]|x_n\rangle$ requires n_x phase shift gates and $n_x(n_x - 1)/2$ controlled phase shift gates. The angles of the phase shift gates are determined by writing $(x_n - 2^{n_x-1})^2 = \sum_{r=0}^{n_x-1} x_n^r (2^{2r} - 2^{n_x+r}) + \sum_{r < s} x_n^r x_n^s 2^{r+s+1} + 2^{2n_x-2}$, where $\{x_n^r\}_{r=0, \overline{n_x-1}}$ is the binary representation of x_n .

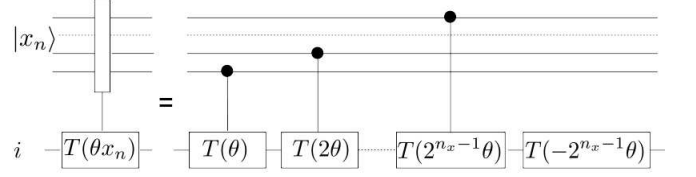


FIG. 3. Circuit for $\exp(-i\theta c_i^\dagger c_i \tilde{X}_n)|i\rangle \otimes |x_n\rangle$. The phase shift angle is $\theta(x_n - N_x/2) = \theta \sum_{r=0}^{n_x-1} x_n^r 2^r - \theta 2^{n_x-1}$, where $\{x_n^r\}_{r=0, \overline{n_x-1}}$ take binary values.

Phonon evolution. Within the Trotter approximation, the algorithm for the evolution of phonons requires the implementation of $\exp(-i\theta\tilde{X}_n^2)|x_n\rangle$, $\exp(-i\theta\tilde{P}_n^2)|x_n\rangle$ and $\exp(-i\theta\tilde{X}_n\tilde{X}_m)|x_n\rangle|x_m\rangle$, where n and m are HO labels.

The implementation of $\exp(-i\theta\tilde{X}_n^2)|x_n\rangle$ requires phase shift gates T and is shown in Fig. 2. The angles of the phase shift gates are determined by writing the eigenvalues of \tilde{X}_n^2 in binary format, as shown in the figure's caption. A phase factor equal to $\exp(i2^{n_x-2}\theta)$ accumulates at each Trotter step. This phase factor can be tracked classically.

For the implementation of $\exp(-i\theta\tilde{P}_n^2)|x_n\rangle$ one first applies a quantum Fourier transform (QFT) [25] $|x_n\rangle \xrightarrow{QFT} |p_n\rangle$, an idea first discussed in Refs. [30, 31]. Then $\exp(-i\theta\tilde{P}_n^2)|p_n\rangle$ is implemented by a circuit similar to the one shown in Fig 2. The last step is an inverse QFT, $|p_n\rangle \xrightarrow{IQFT} |x_n\rangle$.

The operator $\exp(-i\theta\tilde{X}_n\tilde{X}_m)|x_n\rangle|x_m\rangle$ requires two boson registers, n and m . The phase shift angles are determined by writing the product $\tilde{x}_n\tilde{x}_m$ as a sum with binary coefficients [10]. The circuit is similar to the one in Fig. 2. It has n_x^2 controlled phase shift gates and $2n_x$ phase shift gates.

Electron evolution. The algorithm for fermions is described at length in numerous papers (see Refs. [4, 6, 7].) We assume here a Jordan-Wigner mapping of the fermion operators to the Pauli operators X , Y , and Z as in Ref. [7]. Each electron orbital requires a qubit, the state $|\uparrow\rangle \equiv |0\rangle$ ($|\downarrow\rangle \equiv |1\rangle$) corresponding to an unoccupied (occupied) orbital.

Interaction term evolution. The implementation of the electron-phonon interaction is similar to the one for single-particle electron operators which requires phase shift $T(\theta)$ or z-rotations $R_z(\theta)$ gates acting on the electron qubits [6, 7]. The difference is the value of the gate angle θ , which is replaced by $\theta\tilde{x}$, where \tilde{x} is the eigenvalue of \tilde{X} corresponding to the phonon state $|x\rangle$.

In Fig. 3 we show the implementation of $\exp(-i\theta c_i^\dagger c_i \tilde{X}_n)|i\rangle \otimes |x_n\rangle = (T(\theta\tilde{x}_n)|i\rangle) \otimes |x_n\rangle$ where $|i\rangle$ is the i fermion orbital and $|x_n\rangle$ is the state of the HO n .

The circuit for $\exp(-i\theta (c_i^\dagger c_j + c_j^\dagger c_i) \tilde{X}_n)$ (not shown) is similar to the circuit shown in Fig. (9) of Ref. [7] or Table A1 of Ref. [6] for $\exp[-i\theta(c_i^\dagger c_j + c_j^\dagger c_i)]$. The difference is that $R_z(\theta)$ is replaced by $R_z(\theta\tilde{x}_n)$ (see Fig. 8 in Ref. [10]).

The nonlocality of the Jordan-Wigner mapping increases the circuit depth for fermion algorithms [4, 6, 7]. However, the implementation of the electron hopping and electron-phonon terms can be combined. One can implement $\exp[-i(c_i^\dagger c_j + c_j^\dagger c_i)(\theta_0 + \sum_n \theta_n \tilde{X}_n)]$, and there will be no additional Jordan-Wigner strings due to electron-phonon terms. The contribution to the circuit depth for long-range electron-phonon interactions is $\mathcal{O}(N)$.

Input state preparation. The input state for the QPE algorithms must have a large overlap with the ground state. The input state can be obtained by the adiabatic method [32], starting with $H_0 = H_e + H_p$ and slowly turning on the electron-phonon interaction. The ground state of H_0 is $|f_0\rangle \otimes |\Phi_0\rangle$, where $|f_0\rangle$ is the fermion Hamiltonian ground state. Its preparation, while non-trivial, is addressed in the literature [3, 6, 7, 33]. The ground state of H_p is a direct product of grid-projected Gaussian functions $|\chi_0\rangle$, Eq.(9).

Methods to prepare Gaussian states are discussed in Refs. [34, 35]. For the polaron simulations we use the adiabatic method to prepare $|\chi_0\rangle$. Namely, we simulate the time evolution of the state $|x=0\rangle$ under the action of the Hamiltonian $H(\tau) = s(\tau)\tilde{P}^2/2 + \tilde{X}^2/2$ for the annealing time T where $\tau = t/T$. The parameter $s(\tau)$ is varied slowly from zero to one in the time interval T . Because $\tilde{X}^2/2$ has a finite gap of size $\pi/2^{n_x}$, this approach works on small registers [10].

Measurements. Measurements methods described previously [4, 7] can be applied to our algorithm.

Resource scaling. The number of additional qubits required by phonons is $\mathcal{O}(N)$. For finite-range interactions the phonons introduce an $\mathcal{O}(N)$ contribution to the total number of gates and a constant contribution to the circuit depth. For long-range electron-phonon interactions the circuit depth increases linearly with N while the additional number of gates needed is $\mathcal{O}(N^2)$. For long-range phonon-phonon couplings both the additional number of gates and the circuit depth scale as $\mathcal{O}(N^2)$.

Holstein polaron on a quantum simulator. The polaron problem [36], *i.e.*, a single electron interacting

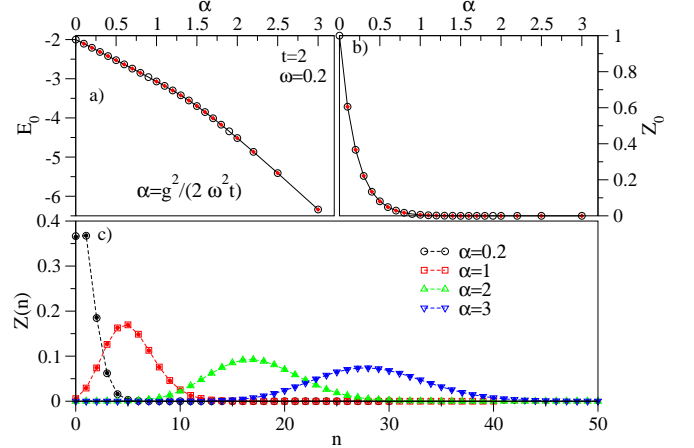


FIG. 4. $n_x = 6$ qubits per HO. The energy (a) and quasiparticle weight (b) for the 2-site Holstein polaron versus coupling strength. (c) The phonon number distribution for different couplings. The open (full) symbols are computed using exact diagonalization (QPE algorithm on a quantum simulator).

with phonons, has been addressed extensively in the literature. In the Holstein model [21] the phonons are described as set of independent oscillators located at every site. The electron density couples locally to the displacement of the HO,

$$H = H_e + g \sum_i c_i^\dagger c_i X_i + \sum_i \frac{P_i^2}{2} + \frac{1}{2} \omega^2 X_i^2. \quad (18)$$

To check the validity of our algorithm we ran a QPE code for the Holstein polaron on a 2-site lattice using an Atos QLM simulator. The 2-site polaron can be solved using the exact diagonalization method on a conventional computer. A comparison between exact diagonalization and our quantum algorithm is shown in Fig. 4. The agreement is good, with a difference of $\mathcal{O}(10^{-4})$ due mainly to the use of the Trotter approximation. We find that $n_x = 6$ qubits for each HO is enough to describe the physics even in the strong coupling regime, which in our case implies a cutoff of $N_{ph} \approx 45$ phonons per site.

In Fig. 4(a) the energy of the polaron as a function of the dimensionless coupling constant $\alpha = g^2/2\omega^2 t$ is plotted. Even this simple 2-site model captures some essential features of more realistic polarons. The transition from light to heavy polarons as a function of the coupling strength is smooth, similar to what is seen in 1D polaron models [37].

The polaron state can be written as $|\Phi\rangle = \sum_{n=0} \sum_r a_{nr} |n, r\rangle$, where $\{|n, r\rangle\}_r$ are normalized vectors spanning the sector with one electron and n phonons. The phonon distribution is defined as $Z(n) = \sum_r |a_{nr}|^2$ and can be determined by applying the QPE algorithm for the phonon evolution Hamiltonian $H_p = \sum_i P_i^2/2 + \omega^2 X_i^2/2$. Since $|\Phi\rangle$ is not an eigenstate of H_p , the energy $E_n = \omega(n+1/2)$ is measured with the probability $Z(n)$.

The quasiparticle weight $Z(0)$ as a function of the coupling strength is shown in Fig. 4 (b). This quantity represents the amount of the free electron in the polaron state and gives the quasiparticle weight measured in the photoemission experiments. In Fig. 4 (c), $Z(n)$ is shown for several values of the coupling strength corresponding to weak, intermediate and strong coupling regimes. The exact diagonalization and the QPE results agree well.

Conclusions. We introduce a quantum algorithm for electron-phonon interacting systems which extends the existing quantum fermion algorithms to include phonons. The phonons are represented as a set of HOs. Each HO space is represented on a finite-sized Hilbert space $\tilde{\mathcal{H}}$. We define operators \tilde{X} and \tilde{P} on $\tilde{\mathcal{H}}$ and show that, in the low-energy subspace, the algebra generated by $\{\tilde{X}, \tilde{P}\}$ is, up to an exponentially small error, isomorphic with the algebra generated by $\{X, P\}$. The size of the low-energy subspace increases approximately linearly with increasing phonon cutoff number N_{ph} . We find that a small number of qubits, $n_x \approx 6, 7$ per HO, is large enough for the simulation of weak, intermediate and strong coupling regimes of most electron-phonons problems of interest.

Our algorithm maps all HO spaces $\tilde{\mathcal{H}}$ on the qubit space and simulates the evolution operator of the electron-phonon Hamiltonian. We present circuits for the implementation of small evolution steps corresponding to different terms in the Hamiltonian. The number of additional qubits required to add phonons is $\mathcal{O}(N)$ where N is proportional to the system size. For long-range interactions, the additional circuit depth and the number of gates due to the phonon inclusion is at worst $\mathcal{O}(N^2)$, while for finite-range interactions the additional circuit depth is constant.

We benchmarked our algorithm on Atos QLM simulator for a two-site Holstein polaron. The polaron energy and phonon distribution are in excellent agreement with the ones calculated by exact diagonalization.

Acknowledgments. We thank Andy Li, Eric Stern, Patrick Fox and Kiel Howe for discussions. This manuscript has been authored by Fermi Research Alliance, LLC under Contract No. DE-AC02-07CH11359 with the U.S. Department of Energy, Office of Science, Office of High Energy Physics. We gratefully acknowledge the computing resources provided and operated by the Joint Laboratory for System Evaluation (JLSE) at Argonne National Laboratory. We would like to thank Atos for the use of their 38-Qubit Quantum Learning Machine (QLM) and support of their universal programming language AQASM.

- [1] Daniel S. Abrams and Seth Lloyd, Phys. Rev. Lett. 79, 2586, (1997).
- [2] Daniel S. Abrams and Seth Lloyd, Phys. Rev. Lett. 83, 5162 (1999).
- [3] G. Ortiz, J. E. Gubernatis, E. Knill, and R. Laflamme, Phys. Rev. A 64, 022319 (2001); Phys. Rev. A 65, 029902, (2002).
- [4] R. Somma, G. Ortiz, J. E. Gubernatis, E. Knill, and R. Laflamme, Phys. Rev. A 65, 042323 (2002).
- [5] Rolando D. Somma, Gerardo Ortiz, Emanuel H. Knill, James Gubernatis, “Quantum simulations of physics problems,” Proc. SPIE 5105, Quantum Information and Computation, (2003).
- [6] James D. Whitfield, Jacob Biamonte and Alan Aspuru-Guzik, “Simulation of electronic structure Hamiltonians using quantum computers,” Molecular Physics Vol. 109, Iss. 5, 2011.
- [7] Dave Wecker, Matthew B. Hastings, Nathan Wiebe, Bryan K. Clark, Chetan Nayak, and Matthias Troyer, Phys. Rev. A **92**, 062318, (2015).
- [8] A. Peruzzo, J. McClean, P. Shadbolt, M.-H. Yung, X.-Q. Zhou, P. J. Love, A. Aspuru-Guzik, and J. L. O’Brien, “A Variational Eigenvalue Solver on a Photonic Quantum Processor,” Nat. Commun. 5, 4213 (2014).
- [9] Jarrod R McClean *et al.*, New J. Phys. 18, 023023, (2016).
- [10] A. Macridin, P. Spentzouris, J. Amundson, R. Harnik, “Digital quantum computation of fermion-boson interacting systems,” arXiv:1805.09928 (2018).
- [11] S. B. Bravyi and A. Y. Kitaev, Ann. Phys. 298, 10 (2002).
- [12] L. A. Wu and D. A. Lidar, “Qubits as parafermions,” Journal of Mathematical Physics 43, 4506 (2002).
- [13] C. D. Batista, G. Ortiz, “Algebraic approach to interacting quantum systems,” Advances in Physics, 53, 1-82, (2007).
- [14] Stephen P. Jordan, Keith S. M. Lee, John Preskill, “Quantum Algorithms for Quantum Field Theories,” Science, Vol. 336, Issue 6085, 1130 (2012).
- [15] C. Clay Marston and Gabriel G. Balint Kurti, “The Fourier grid Hamiltonian method for bound state eigenvalues and eigenfunctions,” The Journal of Chemical Physics 91, 3571 (1989).
- [16] J. C. Light, I. P. Hamilton, and J. V. Lill, “Generalized discrete variable approximation in quantum mechanics,” The Journal of Chemical Physics 82, 1400 (1985).
- [17] Robert G. Littlejohn and Matthew Cargo, “A general framework for discrete variable representation basis sets,” The Journal of Chemical Physics 116, 8691 (2002).
- [18] Aurel Bulgac and Michael McNeil Forbes, “Use of the discrete variable representation basis in nuclear physics,” Phys. Rev. C 87, 051301(R) (2013).
- [19] C.E. Shannon, “Communication in the presence of noise”. Proceedings of the Institute of Radio Engineers, 37, 10, (1949).
- [20] P. Jordan and E. Wigner, Z. Phys. A. 47, 631 (1928).
- [21] T. Holstein, Ann. Phys. (N.Y.) 8, 325 (1959).
- [22] A. Yu. Kitaev, “Quantum measurements and the Abelian Stabilizer Problem,” arXiv:quant-ph/9511026 (1995).
- [23] R. Cleve, A. Ekert, C. Macchiavello, and M. Mosca, Proc. R. Soc. London Sect. A 454, 339354 (1998).
- [24] A. Y. Kitaev, A. H. Shen, and M. N. Vyalyi, “Classical and Quantum Computation,” (American Mathematical Society, Providence, RI, 2002), Vol. 47.
- [25] M. A. Nielsen and I. L. Chuang, “Quantum Computation and Quantum Information,” (Cambridge University Press, Cambridge, UK, 2010).

- [26] Alan Aspuru-Guzik, Anthony D. Dutoi, Peter J. Love, Martin Head-Gordon, *Science*, Vol. 309, 1704, (2005).
- [27] S. Gradshteyn and I. M. Ryzhik, *Tables of Integrals, Series and Products* (Academic, New York, 1965), formula 7.376.
- [28] H. F. Trotter, *Proc. Am. Math. Soc.* 10, 545 (1959).
- [29] M. Suzuki, *Commun. Math. Phys.* 51, 183 (1976).
- [30] Stephen Wiesner, arXiv:quant-ph/9603028, (1996).
- [31] Christof Zalka, “Simulating quantum systems on a quantum computer,” *Proc. Roy. Soc. Lond. A* 454, 313, (1998).
- [32] Farhi, J. Goldstone, S. Gutmann, J. Lapan, A. Lundgren, and D. Preda, *Science* 292, 472 (2001).
- [33] L. A. Wu, M. S. Byrd, and D. A. Lidar, *Phys. Rev. Lett.* 89, 057904 (2002).
- [34] Alexei Kitaev, William A. Webb, “Wavefunction preparation and resampling using a quantum computer,” arXiv:0801.0342, (2008).
- [35] L. K. Grover, T. Rudolph, ”Creating superpositions that correspond to efficiently integrable probability distributions”, arXiv:quant-ph/0208112, (2002).
- [36] L. Landau, *Z. Phys* 3, 664 (1933).
- [37] G. Wellein and H. Fehske, *Phys. Rev. B* 58, 6208 (1998).